Geol. Mag. **155** (*5*), *2018, pp. 1105–1116.* © *Cambridge University Press 2017*

doi:10.1017/S0016756816001278

A revised and improved age model for the middle Miocene part of IODP Site U1318 (Porcupine Basin, offshore southwestern Ireland)

WILLEMIJN QUAIJTAAL*†, STEVEN TESSEUR*, TIMME H. DONDERS‡§, PHILIPPE CLAEYS[|] & STEPHEN LOUWYE*

*Research Unit for Palaeontology, Department of Geology, Ghent University, Krijgslaan 281/S8, 9000 Gent, Belgium
‡Palaeoecology, Department of Physical Geography, Faculty of Geosciences, Utrecht University, Budapestlaan 4, 3584 CD Utrecht, the Netherlands
§TNO B&O, Geological Survey of The Netherlands, PO Box 80015, 3508 TA Utrecht, The Netherlands
[|]Earth System Sciences, Vrije Universiteit Brussel, Pleinlaan 2, 1050 Brussels, Belgium

(*Received* 16 September 2016; *accepted* 12 December 2016; *first published online* 30 January 2017)

Abstract – Integrated Ocean Drilling Program Leg 307 Site U1318 is one of the few relatively complete middle Miocene drillcores from the North Atlantic (Porcupine Basin, offshore southwestern Ireland). Using benthic foraminiferal stable carbon and oxygen isotopes, the existing age model for Site U1318 was improved. The stable isotope record displays globally recognized isotope events, used to revise the existing magnetostratigraphy-based age model. Two intervals contained misidentified magnetochrons which were corrected. The sampled interval now has a refined age of 12.75–16.60 Ma with a temporal resolution of *c.* 29 ka.

Keywords: North Atlantic, isotope stratigraphy, magnetostratigraphy, dinoflagellate cysts, Neogene.

1. Introduction

The middle Miocene period was one of profound climate change (e.g. Flower & Kennett, 1994; Zachos *et al.* 2001). A relatively warm period, the Middle Miocene Climatic Optimum (MMCO; 16–14.5 Ma according to Abels *et al.* 2005; 17–15 Ma according to Shevenell & Kennett, 2004) terminated during the Middle Miocene Climate Transition (MMCT; *c.* 14 Ma, Langhian–Serravallian), the second-largest climate glaciation after the Eocene–Oligocene Transition (Zachos *et al.* 2001). Global comparison between stable isotopic records is essential in understanding the palaeoceanographic and climatic changes during the MMCO and MMCT. Several high-resolution isotope records spanning the MMCO and/or MMCT have become available over the last years, but three large areas remain uncovered: the Indian Ocean, the North Atlantic Ocean and the Arctic Ocean. The Arctic Ocean is extremely difficult to drill, and the few recovered cores have a low recovery (Moran *et al.* 2006). The North Atlantic Ocean has numerous drill sites, however. Nonetheless, the studies from these locations often suffer from hiatuses and generally have a lower resolution than the existing Pacific and Southern Ocean records.

Louwye *et al.* (2008) and Quaijtaal *et al.* (2014) presented palynological data from the Porcupine Basin in the eastern North Atlantic (Fig. 1). Sediments from Integrated Ocean Drilling Program (IODP) Site U1318 are of late early Miocene – middle Miocene age and contained well-preserved organic-walled dinoflagellate cysts (dinocysts) and other marine palynomorphs (Louwye *et al.* 2008). Louwye *et al.* (2008) proposed a first age model for IODP Site U1318 based on magnetostratigraphy, biostratigraphic dinocyst data and the Sr-dating of a mollusc (Kano *et al.* 2007). As reported by Expedition 307 Scientists (2006), the shipboard palaeomagnetic measurements at Site U1318 were affected by magnetic overprint and by noise in the cryogenic magnetometer, rendering the identification of the weak original palaeomagnetic signature difficult. The measured magnetic intensity was considered very low and several measurements have an indistinct inclination between –20° and 20° rather than a distinct value near –90° or 90° (Louwye *et al.* 2008). To overcome these problems, Louwye *et al.* (2008) measured the magnetic signature on several discrete samples since these measurements would not be affected by a magnetic overprint. Quaijtaal *et al.* (2014) updated the age model of Louwye *et al.* (2008) with the aid of additional biostratigraphic dinocyst and calcareous nannoplankton data. However, biostratigraphic tie-points can be diachronic and correlation to global events is necessary to place the 'barcode' of magnetostratigraphy in time correctly.

Here we present new benthic foraminiferal stable carbon and oxygen isotope data from intermediate water depths in the eastern North Atlantic Ocean. These data from a new, relatively complete record fill one of the data gaps in the North Atlantic Ocean. Additionally, the benthic $\delta^{18}O$ and $\delta^{13}C$ stable isotope records

†Author for correspondence: willemijn.quaijtaal@ugent.be

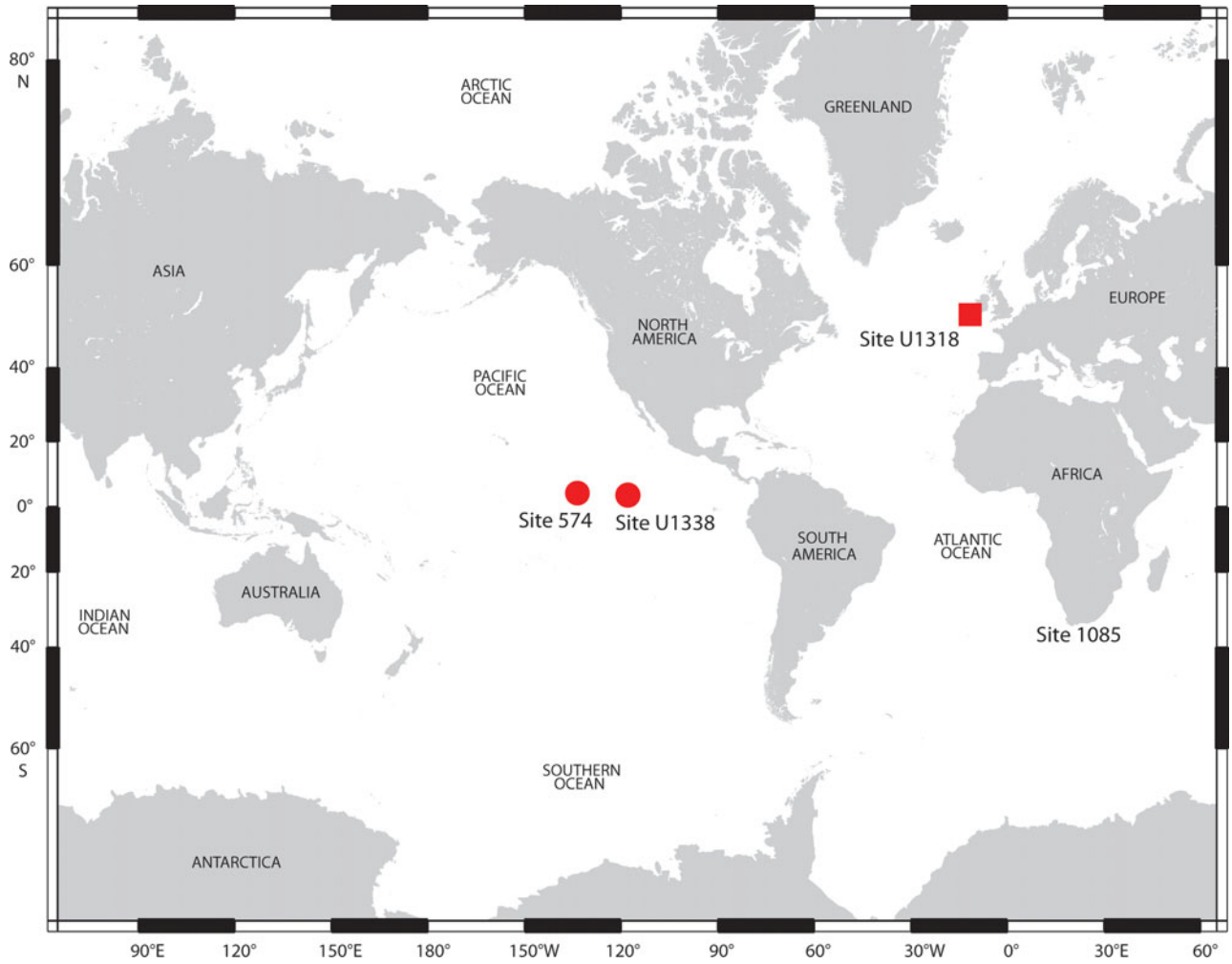

Figure 1. (Colour online) Location of Integrated Ocean Drilling Program (IODP) drill Site U1318, as well as the location of DSDP Site 574 and IODP Site U1338. Figure adapted from IODP drill site maps (http://iodp.tamu.edu/scienceops/maps.html).

presented in this paper aid in confirming or adapting the magnetostratigraphy of Quaijtaal *et al.* (2014) using magnetostratigraphic tie-points provided by Miller, Wright & Fairbanks (1991) and Miller *et al.* (1996, 1998) and globally recognizable isotope stratigraphic events defined by Woodruff & Savin (1991).

2. Material

A total of 145 samples from IODP Leg 307, Site U1318 was selected for stable carbon and oxygen isotope measurements on benthic foraminifera (Fig. 2; online supplementary Table S1, available at http://journals.cambridge.org/geo). Site U1318 (water depth 409 m) was drilled in May 2005 and a composite record was established from Holes U1318B (51° 26.148′ N, 11° 33.019′ W) and U1318C (51° 26.150.4358′ N, 11° 33.040′ W) based on physical properties (Expedition 307 Scientists, 2006). The composite record spans seismic units P1, P2 and P3 (Van Rooij *et al.* 2003) that correspond to (parts of) lithostratigraphic units 1–3. The seismic units and lithostratigraphy are described in more detail in Expedition 307 Scientists (2006) and Quaijtaal *et al.* (2014) (Fig. 2). The samples for this study were selected from lithostratigraphic units 3A, 3B and 3C, which mainly consist of greenish-grey clay and are divided into subunits based on their calcium carbonate contents. Subunit 3A and 3B correspond to seismic unit P2; subunit 3C corresponds to seismic unit P1 (Expedition 307 Scientists, 2006). Sample spacing in the composite record is *c.* 1 m on average.

3. Methodology

3.a. Strategy for isotope analysis

Benthic isotopic records are preferably generated from epifaunal benthic species, since the relative change in $\delta^{13}C$ values of epifaunal foraminifer tests of similar-sized specimens from the same species are dominantly influenced by the $\delta^{13}C$ values of seawater (e.g. Jorissen, 2003; Fontanier *et al.* 2008). The most abundant epifaunal species in the record is *Cibicidoides pachyderma*. This species is morphologically similar to the often-used *C. mundulus* (ex. *C. kullenbergi*) and is known to occur from early Oligocene time until today (Holbourn, Henderson & MacLeod, 2013). Unfortunately *C. pachyderma* was not present in every sample,

https://doi.org/10.1017/S0016756816001278 Published online by Cambridge University Press

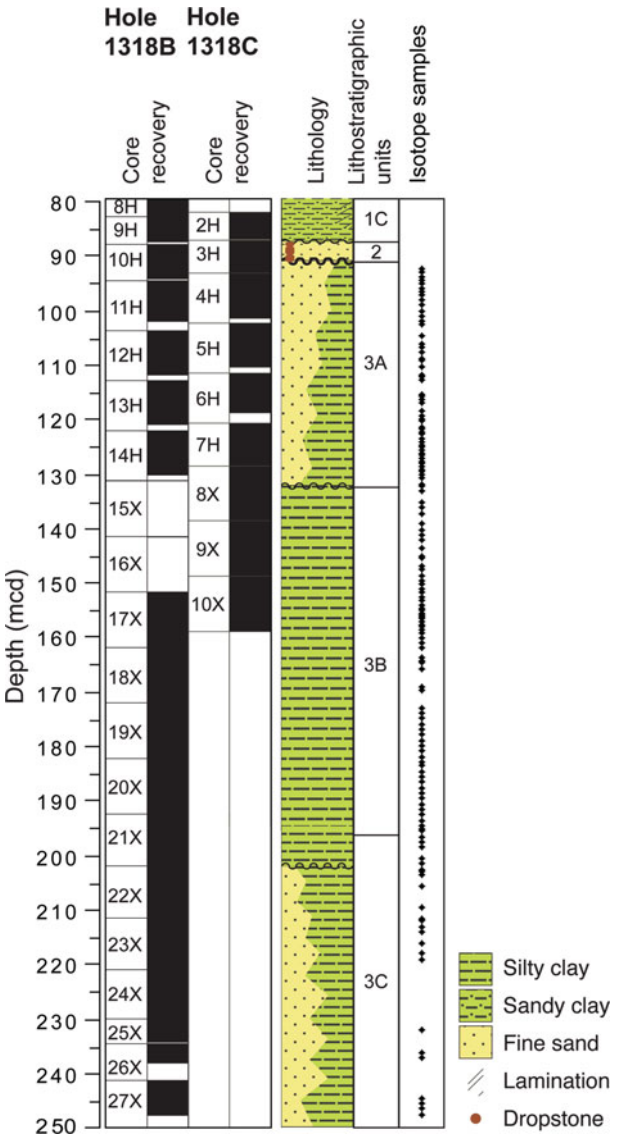

Figure 2. (Colour online) Core recovery (in black), lithology, lithostratigraphy of holes U1318B and U1318C and position of samples analysed for stable isotopes.

and measurements on a mixture of several other epifaunal benthic foraminifera were not justified due to preservational problems. The infaunal taxon *Uvigerina* sp. was therefore selected for measurements in addition to *C. pachyderma*. *Uvigerina* sp. specimens were present almost consistently from 196.54 mcd upwards (Fig. 2; online Supplementary Table S1) with a relatively high abundance and a general good to excellent preservation. The species was absent below 197.59 mcd. The $\delta^{13}C$ value of infaunal species is not only influenced by the $\delta^{13}C$ value of the seawater at a given offset, unlike for epibenthic species, but is also influenced by the microhabitat. In general, a deeper microhabitat results in a more depleted $\delta^{13}C$ signature, which is a potential consequence of the pore-water $\delta^{13}C$ dissolved inorganic carbon (DIC) gradient and/or a consequence of microhabitat effects (McCorkle, Emerson & Quay, 1985; Fontanier *et al.* 2008). Despite this drawback, the advantages of measuring the isotopes on the well-preserved *Uvigerina* sp. specimens is that: (1) preservation issues that could affect the $\delta^{18}O$ values of less-well-preserved *C. pachyderma* specimens (Sexton & Wilson, 2009) can be identified and prevented; and (2) a mixture of epibenthic specimens with possibly different isotope disequilibrium correction factors can be avoided. Changes in the $\delta^{18}O$ values of *Uvigerina* sp. are, as well as the $\delta^{18}O$ values of *C. pachyderma*, expected to reflect changes in the $\delta^{18}O$ value of the seawater (e.g. by glaciation) and the prevailing temperature. There is no known microhabitat influence on the $\delta^{18}O$ isotopes (Fontanier *et al.* 2008).

3.b. Sample preparation and measurements

For isotope measurements the samples were oven dried at 60°C for 24 hours, weighed and subsequently soaked in a tetra-natriumdiphosphat-decahydrat solution (5 g L^{-1}) for at least 24 hours in order to deflocculate the clay (after Snyder & Waters, 1984). The samples were then washed over a sieve with a 63 µm mesh size. The remaining >63 µm fraction was removed from the sieve with distilled water, oven-dried and weighed. The samples were then dry-sieved into three fractions: the 63–180 µm fraction; the 180–250 µm fraction; and the >250 µm fraction. Foraminifera were preferentially picked in the 180–250 µm fraction and complemented with foraminifera from the >250 µm fraction. Two to six specimens (*c.* 40–70 µg) were required for each measurement. The preservation of the picked foraminifera was evaluated relative to each other with the binocular microscope by breaking the foraminifera and assessing the transparency or the fading of textures. The preservation was generally good to moderate for the *C. pachyderma* specimens. Large secondary crystals were never observed with the binocular microscope; scanning electron microscopy showed that some specimens had minor secondary crystals on their test walls, however, which might have influenced the isotopic values (see online Supplementary Plate S1, available at http://journals.cambridge.org/geo). However, there are no indications that the isotopes from these specimens deviate from the others. The *Uvigerina* sp. specimens were generally well preserved.

The $\delta^{18}O$ and the $\delta^{13}C$ stable isotope ratios were measured with a ThermoFinnigan Delta^{plus} XL Mass spectrometer at the Vrije Universiteit Brussel (VUB) in Belgium. This continuous-flow isotope ratio mass spectrometer (CF-IRMS) is equipped with an automated ThermoFinnigan Kiel III carbonate preparation line. Accuracy corrections were made with an in-house standard called Nu Carrara Marble (NCM). The analytical precision averages 0.031 ‰ (1σ) for $\delta^{13}C$ and 0.080 ‰ (1σ) for $\delta^{18}O$. All data (see online Supplementary Table S1) are reported against the Vienna Pee Dee Belemnite (VPDB) standard after calibration of the in-house standard with NBS-19. Duplicate measurements were performed on eight samples. Stable

https://doi.org/10.1017/S0016756816001278 Published online by Cambridge University Press

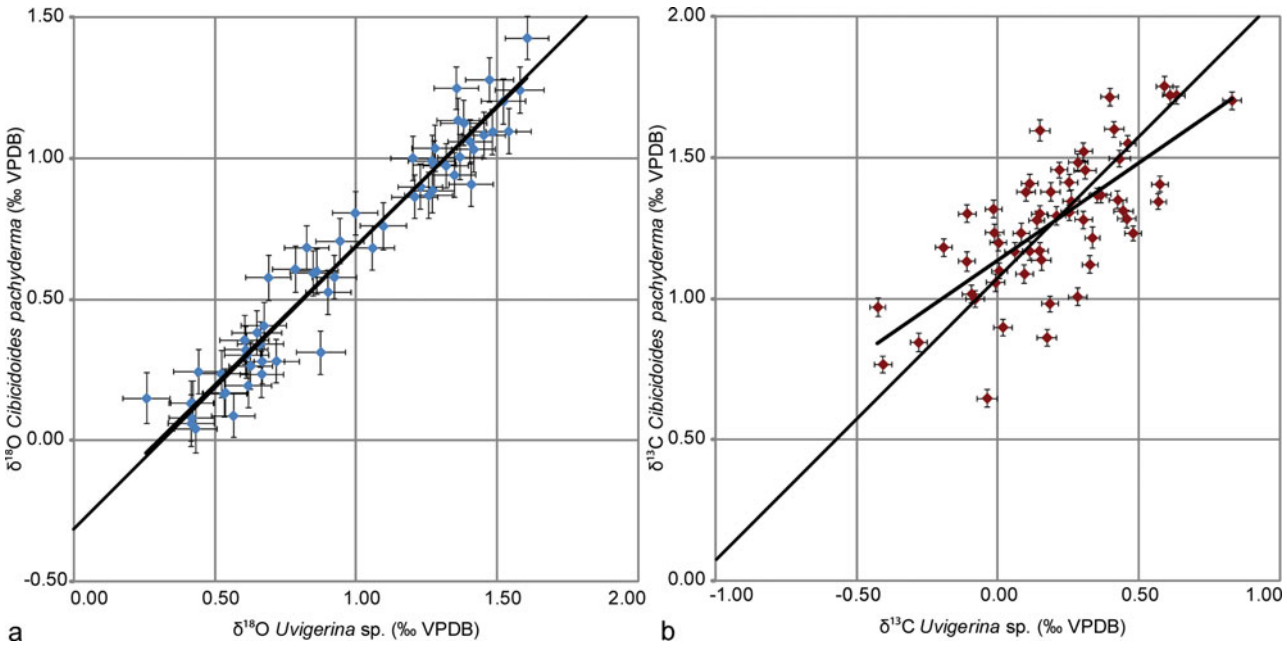

Figure 3. (Colour online) Correlation between uncorrected stable isotope measurements of *C. pachyderma* and *Uvigerina* sp. (a) Correlation of $\delta^{18}O$. The correlation between the two species is $\delta^{18}O_{C.\ pachyderma} = 0.984 \times \delta^{18}O_{Uvigerina\ sp.} - 0.296$ ‰; R^2 is 0.94, prediction error is 0.096 ‰ (1σ, root mean square error of prediction). (b) Correlation of $\delta^{13}C$. The correlation between the two species is $\delta^{13}C_{C.\ pachyderma} = 0.692 \times \delta^{13}C_{Uvigerina\ sp.} + 1.137$ ‰; R^2 is 0.5172, prediction error is 0.170 ‰ (1σ, root mean square error of prediction). Error bars depict one standard deviation (1σ).

isotope data are used here for stratigraphic purposes only.

3.c. Correction factors for isotopic measurements

The $\delta^{13}C$ and $\delta^{18}O$ measurements of modern benthic foraminifera often have a consistent offset from calcite precipitated in equilibrium, and between different species. This is considered a consequence of microhabitat preferences and vital effects (e.g. Katz *et al.* 2003). Despite their different habitat, changes in the $\delta^{18}O$ value of *C. pachyderma* and *Uvigerina* sp. are both expected to reflect the prevailing temperature and the $\delta^{18}O$ value of the seawater at the time of test precipitation. The $\delta^{18}O$ values are therefore assumed to correlate linearly. In 59 samples, both *C. pachyderma* and *Uvigerina* sp. were analysed for stable isotopes. The $\delta^{18}O$ values of both species show a near 1:1 relation (see Fig. 3a). The linear regression resulted in the following equation: $\delta^{18}O_{C.\ pachyderma} = 0.984 \times \delta^{18}O_{Uvigerina\ sp.} - 0.296$ ‰ with a coefficient of determination (R^2) of 0.94 and a prediction error of 0.096 ‰ (1σ, root mean square error of prediction). This good correlation confirms that the $\delta^{18}O$ value of *Uvigerina* sp. can predict the $\delta^{18}O$ value of *C. pachyderma.* The equation can be simplified with the assumption of a slope of 1, which results in the formula: $\delta^{18}O_{C.\ pachyderma} = \delta^{18}O_{Uvigerina\ sp.} - 0.311$ ‰ with a prediction error of 0.097 ‰ (1σ, root mean square error of prediction). This prediction error is considered a consequence of the average analytical precision of 0.080 ‰. The good correlation furthermore suggests that the moderate preservation of some *C. pachyderma* specimens only has a minor or an insignificant impact on the measured $\delta^{18}O$ values in this study.

On the other hand, there is a weaker correlation for $\delta^{13}C$ between *C. pachyderma* and *Uvigerina* sp. (see Fig. 3b). The linear regression resulted in the equation: $\delta^{13}C_{C.\ pachyderma} = 0.692 \times \delta^{13}C_{Uvigerina\ sp.} + 1.137$ ‰ with a coefficient of determination (R^2) of 0.52 and a prediction error of 0.170 ‰ (1σ, root mean square error of prediction). This lower correlation cannot be considered a consequence of preservation since $\delta^{13}C$ has been demonstrated to be more robust to recrystallization than $\delta^{18}O$ (e.g. Sexton, Wilson & Pearson, 2006). The $\delta^{13}C$ values of *Uvigerina* sp. are on average 1.076 ‰ more depleted than the $\delta^{13}C$ values of *C. pachyderma*. This is likely the result of the infaunal habitat of *Uvigerina* sp. Similar offsets of *c.* 0.9 ‰ between *Uvigerina* and *Cibicidoides* were found by Shackleton & Hall (1984) and Shackleton, Hall & Boersma (1984). The lower $\delta^{13}C$ correlation between both taxa is suggested to be a result of the variation of the $\delta^{13}C_{DIC}$ pore-water gradient with time and the possible migration of the infaunal species within the sediment. For correlation of globally recognizable $\delta^{13}C$ maxima, however, this should be of no consequence.

3.d. Isotope stratigraphy

Woodruff & Savin (1991) demonstrated that specific events in the benthic $\delta^{18}O$ and $\delta^{13}C$ isotope records from the Antarctic, Atlantic, Indian and Pacific oceans could be correlated. They defined seven $\delta^{13}C$ maxima (CM1–7) and positive or negative $\delta^{18}O$ excursions

https://doi.org/10.1017/S0016756816001278 Published online by Cambridge University Press

(A–G). They 'relied heavily' (Woodruff & Savin, 1991, p. 762) on the high-resolution isotope record of DSDP Site 574 in the Pacific Ocean to define distinct isotope features. We therefore correlate our $\delta^{13}C$ and $\delta^{18}O$ records of IODP Site U1318 (Porcupine Basin) with the isotopic records of DSDP Site 574 composed of data from Pisias, Shackleton & Hall (1985), Shackleton (unpublished data, 1985, as tabulated by Woodruff & Savin, 1989) and Woodruff & Savin (1989, 1991) using the terminology of Woodruff & Savin (1991), plotted against depth because the initial data were plotted against depth and to avoid problems with different versions of time scales. Furthermore, we include a correlation with IODP Site U1338 in the eastern equatorial Pacific using a recent high-resolution stable isotope study with an astronomically tuned time scale by Holbourn *et al.* (2014). However, the isotope stratigraphy of Woodruff & Savin (1991) is not calibrated against magnetostratigraphy, a correlative tool that is available in the Porcupine Basin (Louwye *et al.* 2008). We have therefore chosen to additionally compare the $\delta^{18}O$ against the Mi-(Miocene isotope) zonation of Miller, Wright & Fairbanks (1991) and Miller *et al*. (1996, 1998) using the updated ages of Boulila *et al.* (2011). The base of these Mi-zones, or Mi-events, is defined by the maximum $\delta^{18}O$ value of one of the originally nine prominent positive $\delta^{18}O$ excursions, possibly related to periods of cryosphere expansion (Miller, Wright & Fairbanks, 1991). By linking the isotope events of Woodruff & Savin (1991) to those of Miller, Wright & Fairbanks (1991) and Miller *et al.* (1996, 1998), we can link our isotope stratigraphy to the correct magnetochron.

4. Results

The isotope stratigraphic correlation between the three compared records is straightforward, despite the fact that IODP Site U1338 and DSDP Site 574 are located in the Pacific Ocean and that IODP Site U1318 is located in the North Atlantic (Fig. 4). If we compare the absolute isotopic $\delta^{18}O$ and $\delta^{13}C$ values between the three records, the $\delta^{18}O$ values from IODP Site U1318 are approximately 1.5 ‰ lower than the $\delta^{18}O$ values of IODP Site U1338 and DSDP Site 574 (Fig. 4). It is assumed that the significantly more depleted $\delta^{18}O$ values in the Porcupine Basin record are mainly a reflection of the warmer temperature conditions as a consequence of the shallower water depth. The absolute $\delta^{13}C$ values of IODP Sites U1318, U1338 and DSDP Site 574 are remarkably similar.

4.a. Determination of isotope stratigraphic tie-points

Discussed from major to minor events, the most prominent event in the record is $\delta^{18}O$ event E, which is defined as an abrupt $\delta^{18}O$ increase of approximately 0.5 ‰. Event E is present in all three records, facilitating further comparison and aiding in the recognition of other isotope stratigraphic tie-points (Fig. 4). At Site U1318, event E can be observed from 143.51 to 133.17 mcd. This event is immediately followed by CM6, subdivided into CM6a and CM6b, at 131.81 and 126.61 mcd, respectively. CM6 is coeval with the base of Mi-zone Mi-3, tied to magnetosubchron C5ABr (Miller, Wright & Fairbanks, 1991). The $\delta^{18}O$ maximum that will be the base of Mi-3 at 128.11 mcd lies just within an interval of normal polarity. According to the age model of Quaijtaal *et al.* (2014) this is C5AAn (Fig. 5), but because of the $\delta^{18}O$ maximum corresponding to Mi-3 it is more likely that this normal subchron represents C5ABn. Chron C5ABr then lies just below Mi-3 in our record, within the undefined polarity interval between 154.85 and 130.02 mcd.

Working downcore, the next stratigraphic tie-point should be CM5. In our record CM5, at *c.* 149.7 mcd, is less pronounced than in the records of DSDP Site 574 and IODP Site U1338 (Fig. 4). A problem with correlating CM5 is that there appear to be three peaks with increased $\delta^{13}C$ values around the interval that Woodruff & Savin (1991) indicated. The middle peak is highest at DSDP Site 574, whereas in IODP Sites U1318 and U1338 the uppermost peak is heaviest. These peaks are tentatively named 5A, 5B and 5C (155.05, 148.51 and 145.51 mcd, respectively, at Site U1318). However, these peaks may also be artefacts of the different resolution between the three records. For depth correlation, the average depth/age value of the three peaks was used.

The next carbon isotope maximum at Site U1318 downcore, CM4, is located at 203.55 mcd (Fig. 4). CM4 appears to be more pronounced at the Porcupine Basin in comparison to the other two records. This $\delta^{13}C$ maximum is higher than CM6, which is not the case in the Pacific records.

The $\delta^{18}O$ event D is less easily characterized. The definition of Woodruff & Savin (1991) states that it is a period of low $\delta^{18}O$ between CM4 and CM5 that is longer in duration than events A–C. However, the interval they appoint to D in their table 11 is rather short. This interval is the first interval of lower $\delta^{18}O$ values, but at both Sites 574 and U1338 five peaks with decreased values follow. At Site U1318 three intervals with lighter values can be found, of which we defined the first as the D-event at 195.03–192.51 mcd (Fig. 4). After this lighter interval at Site U1338, at *c.* 14.7 Ma, a decrease in the amplitude of the $\delta^{18}O$ cycli can be observed (Holbourn *et al.* 2014). This tipping point can also be identified at IODP Site U1318 around *c.* 162 mcd, where the $\delta^{18}O$ minima of the $\delta^{18}O$ cycli decrease from –0.3 ‰ to 0.0 ‰, while the $\delta^{18}O$ maxima remain *c.* 0.5 ‰.

The identification of CM3 is not straightforward. At first the heavy values at *c.* 250–240 mcd were thought to be CM3. However, CM3 is contemporaneous with the base of Mi-zone Mi-2, tied to the base of magnetosubchron C5Br (Miller, Wright & Fairbanks, 1991). According to the age model of Quaijtaal *et al.* (2014) the initial interval for CM3 should correspond

https://doi.org/10.1017/S0016756816001278 Published online by Cambridge University Press

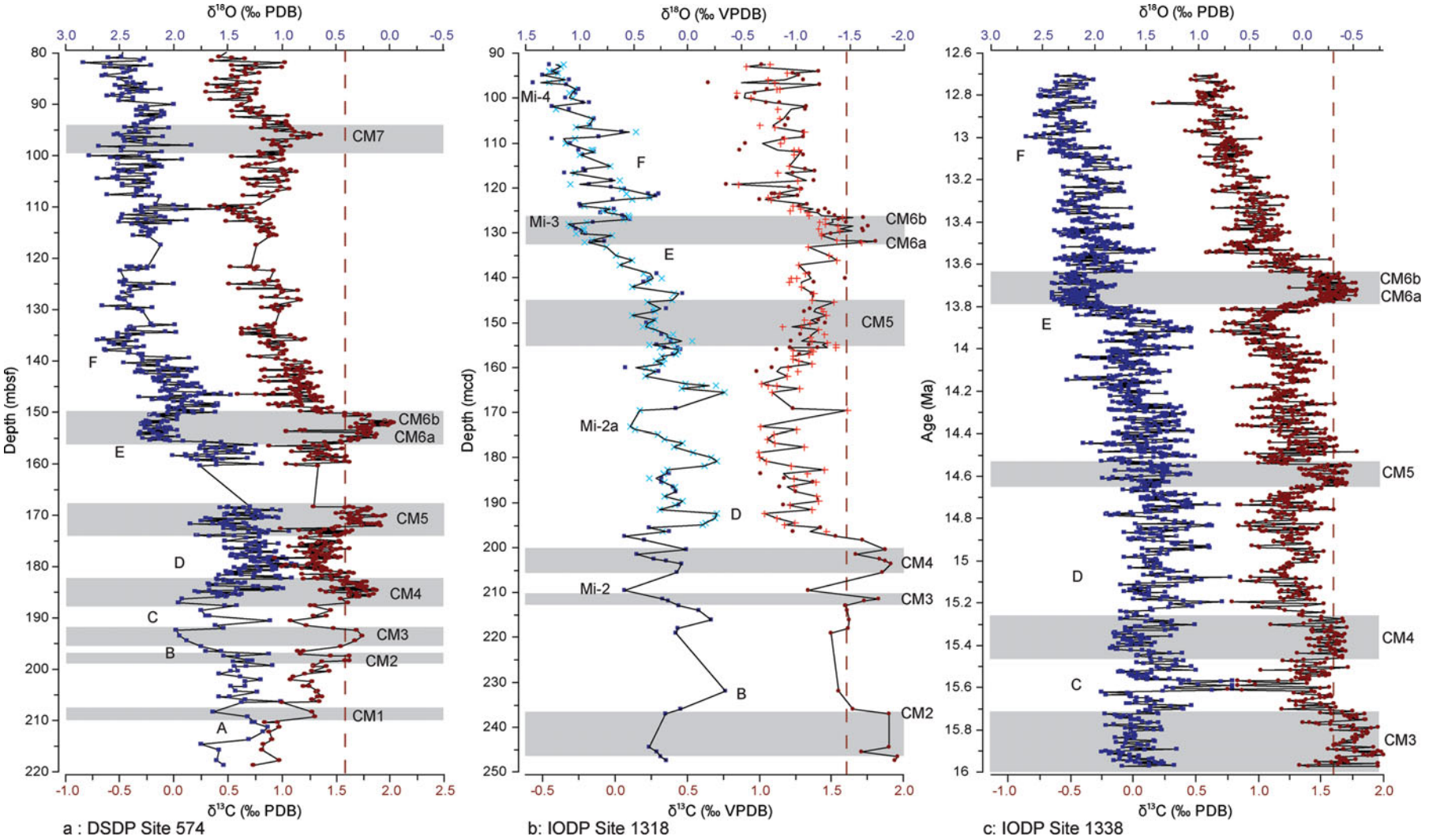

Figure 4. (Colour online) Stable benthic oxygen ($\delta^{18}O$) and carbon isotopes ($\delta^{13}C$). Oxygen isotopes are represented by blue squares, carbon isotopes by red dots. The red dashed line is the CM line of 1.6 ‰ from Woodruff & Savin (1991) as set from Site 574. (a) Isotopes from DSDP Site 574 versus depth (Pisias, Shackleton & Hall, 1985; Woodruff & Savin, 1989; Woodruff & Savin, 1991; Shackleton, unpublished data tabulated by Woodruff & Savin, 1989). $\delta^{13}C$ values were not corrected for vital effects. (b) Isotopes from IODP Site U1318 versus depth. Dark blue squares and dark red dots are uncorrected measurements on *C. pachyderma*, light blue crosses and red plus signs are corrected measurements on *Uvigerina* sp. using the following formulas: $\delta^{18}O_{C.\ pachyderma} = 0.984 \times \delta^{18}O_{Uvigerina\ sp.} - 0.296$ ‰; $\delta^{13}C_{C.\ pachyderma} = 0.692 \times \delta^{13}C_{Uvigerina\ sp.} + 1.137$ ‰. (c) Isotopes from IODP Site U1338 versus age. Data from Holbourn *et al.* (2014). $\delta^{13}C$ values were not corrected for vital effects.

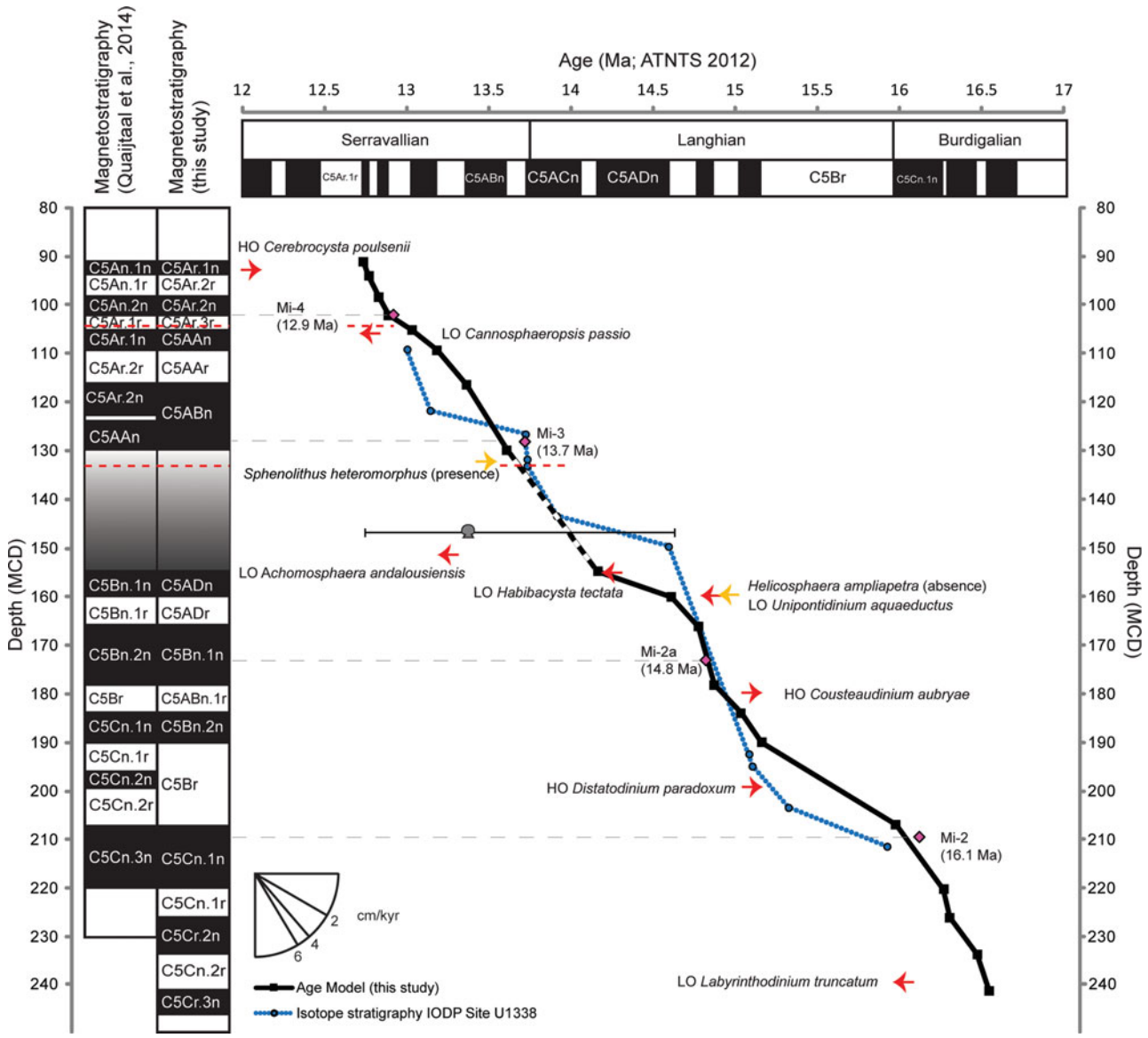

Figure 5. (Colour online) Updated age model for IODP Site U1318 (in black); the tie-points based on the isotope stratigraphy of Site 1338 (in blue). Pink diamonds represent the Mi-events versus depth at Site U1318 and ages from Boulila *et al.* (2011), connected to the magnetostratigraphy at Site U1318 with grey dashed lines. The black dashed line indicates the interval where ages were interpolated because of the uncertainty in the magnetostratigraphy. Black squares are magnetostratigraphic tie-points, red dashed lines indicate hiatuses, red arrows indicate dinocyst biostratigraphic tie-points, yellow arrows indicate nannoplankton presence or absence, grey mollusc indicates Sr-isotopic age from Kano *et al.* (2007).

to subchron C5Cr.3n, and the base of C5Br should be at 184.15 mcd (Fig. 5). However, at the latter depth no clear δ^{18}O maximum and corresponding carbon isotope maximum can be observed. Another carbon isotope maximum can be observed just directly below CM4 at 211.57 mcd. This maximum is close to a δ^{18}O maximum at 209.55 mcd, and just below an interval of reversed polarity. Although this does not fit the description of Mi-2 entirely, the resolution of the isotope records in this interval is somewhat lower than higher up the composite record and it is to be expected that the highest maxima lie within the non-sampled part. We therefore tentatively appoint a depth of 211.57 mcd to CM3 and a depth of 209.55 mcd to Mi-2. There are no decreased δ^{18}O values between CM3 and CM4, implying that isotope event C of Woodruff & Savin (1991) is not present in the Porcupine Basin. This event however is 'often exhibited as a single data point' (Woodruff & Savin, 1991) and it might therefore be missing due to the lower sampling resolution in this part of the composite.

Due to the successful identification of Mi-zones Mi-2 and Mi-3, zone Mi-2a could also be identified. According to Miller *et al.* (1998) zone Mi-2a is tied to the base of magnetosubchron C5ADr. The fourth reversal above 207.15 mcd (base C5Br according to the location of Mi-2) is at 166.25 mcd (Fig. 4). There are two δ^{18}O maxima surrounding this point, at 159.98 mcd and 173.08 mcd. Both points are located within an interval of normal polarity, contradictory to the

https://doi.org/10.1017/S0016756816001278 Published online by Cambridge University Press

indication of Miller *et al.* (1998). We have tentatively placed Mi-2a at 173.08 mcd because of the slightly heavier $\delta^{18}O$ values.

The remaining CM at 237.1 mcd in IODP Site U1318 is CM2 (Fig. 4). It is plausible that the low $\delta^{18}O$ value at *c.* 232.045 mcd then corresponds to $\delta^{18}O$-event B, although this depth should be treated with care since this is a single measurement and the resolution between 220 mcd and 240 mcd is very low.

The remaining $\delta^{18}O$ event of Woodruff & Savin (1991) is event F. This event is coeval with the base of Mi-zone Mi-4 at the base of (undivided) C5Ar (Miller, Wright & Fairbanks, 1991). Several $\delta^{18}O$ maxima are present above the base of zone Mi-3 at the Porcupine Basin. The fourth reversal above the top of C5ABr/base of C5ABn (as indicated by the location of Mi-3) should mark the base of C5Ar, the location of Mi-4 according to Miller, Wright & Fairbanks (1991) and Miller *et al.* (1998), and is located at 116.51 mcd (Figs 4, 5). Around that depth a smaller $\delta^{18}O$ maximum can be observed. However, according to Holbourn *et al.* (2005, 2007) and Holbourn *et al*. (2013), there is an interval of dominance of the 100 ka eccentricity cycle during 13.5–13.1 Ma, which at the Porcupine Basin should be between *c.* 128 and 102 mcd (13.1–12.5 Ma according to Quaijtaal *et al.* 2014; A. Holbourn, pers. comm., 2016). The $\delta^{18}O$ maximum at the end of this eccentricity-dominated interval should mark Mi-4, and we place the base of zone Mi-4 at 101.95 mcd. Isotope event F spans 121.76–109.11 mcd. Event F is defined as the start of an episode of maximum middle Miocene $\delta^{18}O$ values (Woodruff & Savin, 1991). It also corresponds to one of the major incremental steps of increasing $\delta^{18}O$ values and decreasing amplitude in the $\delta^{18}O$ variability recognized by Holbourn *et al.* (2007). Furthermore, the relative increase in $\delta^{18}O$ maxima after $\delta^{18}O$ event E and F is approximately 0.3 ‰ in all three records.

4.b. Revision of the age model

The astronomically tuned isotopic events recognized at IODP Site 1338 provide a first approximate age for the corresponding events at IODP Site U1318 (see Table 1). According to the isotope stratigraphy, the record at IODP site U1318 encompasses a time interval from somewhat older than 16 Ma to somewhat younger than 13 Ma (Figs 4, 5); this is in contrast to the age model of Quaijtaal *et al.* (2014) that suggests a time interval from *c.* 17.8 Ma to 12.0 Ma. The approximate ages provided by the isotope stratigraphy correspond better with three biostratigraphic dinocyst ages in the lower part of the record (Fig. 5). The highest occurrence of *Cousteaudinium aubryae* and *Distatodinium paradoxum* were calibrated against the top of magnetosubchron C5Br (De Verteuil & Norris, 1996), now at an age of 15.16 Ma (ATNST 2012). The lowest occurrence of *Labyrinthodinium truncatum* at 237 mcd, in the bottom part of the record, is correlated against the Burdigalian–Langhian boundary according to Williams *et al.* (2004). This boundary is currently dated at 15.97 Ma, supported by a Sr-isotope dating of <16.6 Ma by Dybkjaer & Piasecki (2010).

The first direct tie-points for magnetostratigraphy were provided by the base of Mi-zones (Table 2, Fig. 5). The identification of the base of Mi-2 led to the interpretation of the reversal at 207.15 mcd as the boundary between magnetosubchrons C5Cn.1n and C5Br. Mi-2a provided the identification of the boundary between C5Bn.1n and C5ADr at 166.25 mcd. This indicates that the age model of Quaijtaal *et al.* (2014) is one magnetochron too old during Mi-2a and two magnetochrons too old during Mi-2. Above the undefined polarity interval between 154.85 and 130.02 mcd we can identify the boundary between C5ABr and C5ABn at 130.02 mcd due to the position of Mi-3 at 128.11 mcd. The boundary between C5Ar.2n and C5Ar.3r could be identified because of Mi-4. The age model of Quaijtaal *et al.* (2014) is one magnetochron too young for the interval spanning Mi-3, and two magnetochrons too young during Mi-4.

The combination of offsets between the different magnetochrons and the differential offsets between the Mi-events indicate that a simple shift in magnetochrons would not provide a solution; we have therefore carefully studied the inclination data of Site U1318. From *c.* 160 mcd downwards, the divergence between the bio- and isotope stratigraphic tie-points and the age model of Quaijtaal *et al.* (2014) becomes largest. When restudying the inclination data, it appeared that the signal of the discrete samples of Louwye *et al.* (2008) in the interval between 207.15 and 190.15 mcd is quite irregular (see their fig. 8). Louwye *et al.* (2008) interpreted this interval as three magnetosubchrons: C5Bn.1r, C5Bn.2n and C5Br. The interpretation of C5Bn.2n is based on two discrete measurements. However, the surrounding measurements are relatively scattered, whereas in most subchrons the measurements tend to cluster together. We have therefore reinterpreted this interval as being one magnetosubchron: C5Br. This reinterpretation is compatible with the isotope stratigraphy, and the longer duration of magnetosubchron C5Br fits better with the sediment thickness (17 m). From the base of the composite record up to 207.15 mcd, the magnetostratigraphy was therefore shifted by two chrons towards a younger age; from 190.15 up to 154.85 mcd, age was shifted one chron upwards.

The interval between 154.85 and 130.02 mcd proves to be more difficult due to the lack of discrete samples, as well as the hiatus at 133.2 mcd. We have therefore linearly interpolated between the two assigned reversals encompassing this interval.

For the interval from 130.02 mcd to the top of the composite record, we used the same approach as in the interval below 154.85 mcd. Re-evaluation of the inclination data showed that the short reversed

https://doi.org/10.1017/S0016756816001278 Published online by Cambridge University Press

Table 1. Depths and ages of the isotope stratigraphic events of Woodruff & Savin (1991) for DSDP Site 574, IODP Site U1318 and IODP Site 1338.

Selected isotope stratigraphy events (Woodruff & Savin, 1991)	DSDP Site 574 Depth (mbsf)	IODP Site U1338		IODP Site U1318	
		Depth (mcd)	Age (Ma)	Depth (mcd)	Age (Ma, ATNTS 2012)
CM1	209.31	N/A	N/A	N/A	N/A
CM2	197.4	N/A	N/A	237.085	16.50
CM3	193.46	433.56	15.92	211.57	16.07
CM4	184.71	414.67	15.32	203.55	15.80
CM5A	172.11	395.63	14.62	155.05	14.18
CM5B	170.01	394.13	14.58	148.51	14.02
CM5C	168.71	392.98	14.55	145.51	13.95
CM5 (average)	170.28	394.25	14.59	149.69	14.05
CM6A	154.31	366.13	13.73	131.81	13.65
CM6B	152.01	365.58	13.72	126.61	13.55
CM7	95.89 (?)	N/A	N/A	N/A	N/A
δ^{18}O Event A	213.71–210.31	N/A	N/A	N/A	N/A
δ^{18}O Event B	196.97	N/A	N/A	232.045	16.43
δ^{18}O Event C	190.55	424.84–423.84	15.61–15.57	N/A	N/A
δ^{18}O Event D	179.91–179.37	409.60–409.00	15.10–15.08	195.03–192.51	15.39–15.27
δ^{18}O Event E	156.31–155.31	373.09–366.33	13.91–13.73	143.51–133.17	13.91–13.68
δ^{18}O Event F	138.43–137.82	345.71–339.58	13.14–13.0	121.76–109.11	13.46–13.17

Table 2. Ages, corresponding magnetosubchrons and depths of the Mi-zones of Miller, Wright & Fairbanks (1991) and Miller *et al.* (1998). First ages and magnetosubchrons according to Boulila *et al.* (2011), Miller, Wright & Fairbanks (1991) and Miller *et al.* (1998), following depths, ages and magnetosubchrons according to this study.

Mi-zone	Age (Ma)	Magnetosubchron	Depth (mcd)	Age (Ma; ATNTS 2012)	Magnetosubchron
Source	Boulila *et al.* (2011)	Miller, Wright & Fairbanks (1991); Miller *et al.* (1998)	Site U1318	Site U1318	Site U1318
Mi-4	12.9	base C5Ar	101.95	12.88	base C5Ar.2n
Mi-3	13.7	C5ABr	128.11	13.57	base C5ABn
Mi-2a	14.8	base C5ADr	173.08	14.83	C5Bn.1n
Mi-2	16.1	base C5Br	209.55	16.03	top C5Cn.1n

interval between 124.32 and 122.81 mcd is misinterpreted. The discrete measurements show no sign of any reversals, and most on-board measurements point towards a normal polarity. We therefore interpret the interval from 130.02 to 116.51 mcd as one instead of three magnetosubchrons. Aided by the location of the Mi-events and their corresponding magnetosubchrons, from 130.02 to 116.51 mcd age was shifted one magnetochron towards older age, and from 116.15 mcd to the top of the composite record age was shifted two magnetochrons towards older age. This implies that the interval between 154.85 and 130.02 mcd contains three magnetosubchrons (Fig. 5).

An overview of all tie-points can be found in Table 3 and a visualization of the new age model is displayed in Figure 5.

5. Discussion and conclusions

With the aid of stable isotope stratigraphy we have been able to refine the age model for IODP Site U1318. The sampled interval now encompasses an age of 12.75–16.60 Ma; the average sampling resolution of our stable isotope record with the new age model is *c.* 29 ka. The estimated duration of the hiatus over 104.60–104.31 mcd is estimated at *c.* 32 ka. Due to the uncertainties in the magnetostratigraphy over 154.85–130.02 mcd, the duration of the hiatus at 133.20 mcd cannot be determined and the model was linearly interpolated up- and downwards.

Sedimentation rates vary from *c.* 1.2 to 16.9 cm ka^{-1}. The record can roughly be divided into five sections. The first section, 241.45–207.15 mcd, has an average sedimentation rate of 6.03 cm ka^{-1} and ends shortly after Mi-2. Sedimentation rates decrease to 2.6 cm ka^{-1} on average over 207.5–178.35 mcd. Between 178.35 and 160.15 mcd rates increase to *c.* 6.9 cm ka^{-1}. For the fourth section (160.15–130.02 mcd) the average sedimentation of *c.* 3 cm ka^{-1} is a rough estimate, since the age model was linearly interpolated between two recognizable magnetic reversals. The last section (130.02–91.44 mcd) has relatively constant sedimentation rates of *c.* 4.45 cm ka^{-1}.

The Porcupine Basin benthic foraminiferal stable isotope records show clear imprints of globally recognized stable isotope events and have a relatively large temporal range; they will therefore be significant for further interbasinal comparisons and correlations with surface ocean parameters to elucidate triggers and drivers for Miocene climatic transitions. Some of these stable isotope events were used as guidelines for the correct identification of palaeomagnetic reversals. The other points were compared to the astronomically tuned high-resolution record from IODP Site 1338, and used to improve the age model

https://doi.org/10.1017/S0016756816001278 Published online by Cambridge University Press

Table 3. Magnetostratigraphic and biostratigraphic tie-points for Site U1318. Tie-points in bold are used to generate the age model.

Bio- /magnetostratigraphic event	Age (Ma)	Site	Palaeomagnetic interpretation		Reference for age
			Depth (mbsf)	Depth (mcd)	
Top C5An.1n	**12.049**		N/A	N/A	**ATNTS 2012**
HO *Cerebrocysta poulsenii* (Quaijtaal *et al.* 2014)	12.1	1318B	87.795	92.735	Schreck, Matthiessen & Head (2012)
Bottom C5An.1n	**12.174**		N/A	N/A	**ATNTS 2012**
Top C5An.2n	**12.272**	**1318B**	N/A	N/A	**ATNTS 2012**
Bottom C5An.2n	**12.474**	**1318B**	N/A	N/A	**ATNTS 2012**
LO *Cannosphaeropsis passio* (Quaijtaal *et al.* 2014)	12.73	1318B	101.565	105.875	Hilgen *et al.* (2012)
Top C5Ar.1n	**12.735**	**1318B**	**86.2**	**91.14**	**ATNTS 2012**
Bottom C5Ar.1n	**12.77**	**1318B**	**89.1**	**94.04**	**ATNTS 2012**
Top C5Ar.2n	**12.829**	**1318C**	**94**	**98.43**	**ATNTS 2012**
Bottom C5Ar.2n	**12.887**	**1318C**	**97.8**	**102.23**	**ATNTS 2012**
Top Hiatus 1				**104.31**	**Linear interpolation**
Bottom Hiatus 1				**104.60**	**Linear interpolation**
Top C5AAn	**13.032**	**1318C**	**99.1**	**105.2**	**ATNTS 2012**
Bottom C5AAn	**13.183**	**1318B**	**103.3**	**109.4**	**ATNTS 2012**
LO *Achomosphaera andalousiensis* (unpublished)	13.2	1318C	145.5	151.405	Hilgen *et al.* (2012)
Top C5ABn	**13.363**	**1318B**	**110.8**	**116.51**	**ATNTS 2012**
Sr-dated mollusc fragment	(12.74) 13.381 (14.624)	1318C	140.83	146.74	Kano *et al.* (2007)
Presence *Sphenolithus heteromorphus* (Quaijtaal *et al.* 2014)	>13.52	1318C	127.29	131.81	Hilgen *et al.* (2012)
Bottom C5ABn	**13.608**	**1318B**	**125.5**	**130.02**	**ATNTS 2012**
Top Hiatus 2				**133.20**	
Bottom Hiatus 2				**133.20**	
Top C5ACn	13.739		N/A	N/A	ATNTS 2012
Bottom C5ACn	14.07		N/A	N/A	ATNTS 2012
Top C5ADn	**14.163**	**1318B**	**148.7**	**154.85**	**ATNTS 2012**
LO *Habibacysta tectata* (unpublished)	14.2	1318B	149.05	155.1	Schreck, Matthiessen & Head (2012)
Bottom C5ADn	**14.609**	**1318B**	**154.2**	**160.15**	**ATNTS 2012**
Top C5Bn.1n	**14.775**	**1318B**	**160.1**	**166.25**	**ATNTS 2012**
LO *Unipontidinium aquaeductus* (unpublished)	14.8	1318C	153.765	159.815	Dybkjaer & Piasecki (2010)
Bottom C5Bn.1n	**14.87**	**1318B**	**172.2**	**178.35**	**ATNTS 2012**
Absence *Helicosphaera ampliaperta* (Quaijtaal *et al.* 2014)	<14.91	1318C	153.7	159.65	Hilgen *et al.* (2012)
Top C5Bn.2n	**15.032**	**1318B**	**178**	**184.15**	**ATNTS 2012**
Bottom C5Bn.2n	**15.16**	**1318B**	**184**	**190.15**	**ATNTS 2012**
HO *Cousteaudinium aubryae* (unpublished)	15.16	1318B	173.72	179.87	De Verteuil and Norris (1996)
HO *Distatodinium paradoxum* (Louwye *et al.* 2008)	15.16	1318B	193.155	199.305	De Verteuil and Norris (1996)
LO *Labyrinthodinium truncatum* (Louwye *et al.* 2008)	15.97	1318B	233.415	239.565	Dybkjaer and Piasecki (2010)
Top C5Cn.1n	**15.974**	**1318B**	**201**	**207.15**	**ATNTS 2012**
Bottom C5Cn.1n	**16.268**	**1318B**	**214.3**	**220.45**	**ATNTS 2012**
Top C5Cn.2n	**16.303**	**1318B**	**220.1**	**226.35**	**ATNTS 2012**
Bottom C5Cn.2n	**16.472**	**1318B**	**227.8**	**233.95**	**ATNTS 2012**
Top C5Cn.3n	**16.543**	**1318B**	**235.3**	**241.45**	**ATNTS 2012**

for IODP Site U1318 further. Furthermore, the oxygen isotope measurements on benthic foraminifer species *Cibicidoides pachyderma* and *Uvigerina* sp. correlate very well. Measurements on *Uvigerina* sp. can be converted to *Cibicidoides* using the following formula: $\delta^{18}O_{Cibicidoides\ pachyderma} = 0.984 \times \delta^{18}O_{Uvigerina\ sp.} - 0.296‰$ ($R^2 = 0.94$), prediction error 0.096‰ (1σ, root mean square error of prediction).

Acknowledgements. The data used for this study can be found in online Supplementary Table S1 (available at http://journals.cambridge.org/geo). The samples for this study were provided by the Integrated Ocean Drilling Program. This work was supported by the Research Foundation-Flanders (FWO) under project number G.0179.11N. Ph.C. thanks the Hercules Foundation Flanders for support of the Stable Isotope facility. The advice of Dr An Holbourn on Miocene stable oxygen isotopes was very valuable for the improvement of the age model. Niels de Winter is thanked for his support during the isotopic measurements in Brussels. Walter Hale and Alex Wülbers kindly supported W.Q. and S.L. during sampling at the Bremen Core Repository. The authors thank Dirk Munsterman and one anonymous reviewer for their useful comments, which have improved the manuscript.

Declaration of interest

The authors declare no conflicts of interest.

https://doi.org/10.1017/S0016756816001278 Published online by Cambridge University Press

Supplementary material

To view supplementary material for this article, please visit https://doi.org/10.1017/S0016756816001278.

References

Abels, H. A., Hilgen, F. J., Krijgsman, W., Kruk, R. W., Raffi, I., Turco, E. & Zachariasse, W. J. 2005. Long-period orbital control on middle Miocene global cooling: Integrated stratigraphy and astronomical tuning of the Blue Clay Formation on Malta. *Paleoceanography* **20**(4), PA4012.

Boulila, S., Galbrun, B., Miller, K. G., Pekar, S. F., Browning, J. V., Laskar, J. & Wright, J. D. 2011. On the origin of Cenozoic and Mesozoic 'third-order' eustatic sequences. *Earth-Science Reviews* **109**(3–4), 94–112.

De Verteuil, L. & Norris, G. 1996. Miocene dinoflagellate stratigraphy and systematics of Maryland and Virginia. *Micropaleontology, supplement* **42**, 1–172.

Dybkjaer, K. & Piasecki, S. 2010. Neogene dinocyst zonation for the eastern North Sea Basin, Denmark. *Review of Palaeobotany and Palynology* **161**(1–2), 1–29.

Expedition 307 Scientists 2006. Site U1318. In *Proceedings of the Integrated Ocean Drilling Program* (eds T. G. Ferlman, A. Kano, T. Williams, J.-P. Henriet & the Expedition 307 Scientists), pp. 1–57. Washington, DC: Integrated Ocean Drilling Program Management International.

Flower, B. P. & Kennett, J. P. 1994. The middle Miocene climatic transition: East Antarctic ice sheet development, deep ocean circulation and global carbon cycling. *Palaeogeography, Palaeoclimatology, Palaeoecology* **108**(3–4), 537–55.

Fontanier, C., Jorissen, F. J., Michel, E., Cortijo, E., Vidal, L. & Anschutz, P. 2008. Stable oxygen and carbon isotopes of live (stained) benthic foraminifera from Cap-Ferret Canyon (Bay of Biscay). *The Journal of Foraminiferal Research* **38**(1), 39–51.

Hilgen, F.J., Lourens, L.J., Van Dam, J.A., Beu, A.G., Boyes, A.F., Cooper, R.A., Krijgsman, W., Ogg, J.G., Piller, W.E. & Wilson, D.S. 2012. The Neogene Period. In *The Geologic Time Scale* (eds. F. M. Gradstein, J. G. O. D. Schmitz & G. M. Ogg), pp. 923–978. Boston: Elsevier.

Holbourn, A., Henderson, A. S. & MacLeod, N. 2013. A to V. In *Atlas of Benthic Foraminifera*, pp. 15–615. Oxford, UK: Wiley-Blackwell.

Holbourn, A., Kuhnt, W., Frank, M. & Haley, B. A. 2013. Changes in Pacific Ocean circulation following the Miocene onset of permanent Antarctic ice cover. *Earth and Planetary Science Letters* **365**, 38–50.

Holbourn, A., Kuhnt, W., Lyle, M., Schneider, L., Romero, O. & Andersen, N. 2014. Middle Miocene climate cooling linked to intensifi cation of eastern equatorial Pacific upwelling. *Geology* **42**(1), 19–22.

Holbourn, A., Kuhnt, W., Schulz, M. & Erlenkeuser, H. 2005. Impacts of orbital forcing and atmospheric carbon dioxide on Miocene ice-sheet expansion. *Nature* **438**(7067), 483–7.

Holbourn, A., Kuhnt, W., Schulz, M., Flores, J. A. & Andersen, N. 2007. Orbitally-paced climate evolution during the middle Miocene 'Monterey' carbon-isotope excursion. *Earth and Planetary Science Letters* **261**(3–4), 534–50.

Jorissen, F. J. 2003. Benthic foraminiferal microhabitats below the sediment-water interface. In *Modern Foraminifera* (ed. B. K. Sen Gupta), pp. 161–79. Dordrecht: Springer Netherlands.

Kano, A., Ferdelman, T. G., Williams, T., Henriet, J. P., Ishikawa, T., Kawagoe, N., Takashima, C., Kakizaki, Y., Abe, K., Sakai, S., Browing, E. L., Li, X., Andres, M. S., Bjerager, M., Cragg, B. A., De Mol, B., Dorschel, B., Foubert, A., Frank, T. D., Fuwa, Y., Gaillot, P., Gharib, J. J., Gregg, J. M., Huvenne, V. A. I., Léonide, P., Mangelsdorf, K., Monteys, X., Novosel, I., O'Donnell, R., Rüggeberg, A., Samarkin, V., Sasaki, K., Spivack, A. J., Tanaka, A., Titschack, J., van Rooij, D. & Wheeler, A. 2007. Age constraints on the origin and growth history of a deep-water coral mound in the northeast Atlantic drilled during Integrated Ocean Drilling Program Expedition 307. *Geology* **35**(11), 1051–4.

Katz, M. E., Katz, D. R., Wright, J. D., Miller, K. G., Pak, D. K., Shackleton, N. J. & Thomas, E. 2003. Early Cenozoic benthic foraminiferal isotopes: Species reliability and interspecies correction factors. *Paleoceanography* **18**(2), doi:10.1029/2002PA000798.

Louwye, S., Foubert, A., Mertens, K., Van Rooij, D. & The IODP Expedition 307 Scientific Party 2008. Integrated stratigraphy and palaeoecology of the Lower and Middle Miocene of the Porcupine Basin. *Geological Magazine* **145**, 321–44.

McCorkle, D. C., Emerson, S. R. & Quay, P. D. 1985. Stable carbon isotopes in marine porewaters. *Earth and Planetary Science Letters* **74**(1), 13–26.

Miller, K. G., Mountain, G. S., Browning, J. V., Kominz, M., Sugarman, P. J., Christie-Blick, N., Katz, M. E. & Wright, J. D. 1998. Cenozoic global sea level, sequences, and the New Jersey Transect: Results fom coastal plain and continental slope drilling. *Reviews of Geophysics* **36**(98), 569–601.

Miller, K. G., Mountain, , G. S., the Leg 150 Shipboard Party & Members of the New Jersey Coastal Plain Drilling Project 1996. Drilling and dating New Jersey Oligocene–Miocene sequences: ice volume, global sea level, and Exxon records. *Science* **271**(5252), 1092–5.

Miller, K. G., Wright, J. D. & Fairbanks, R. G. 1991. Unlocking the ice house: Oligocene-Miocene oxygen isotopes, eustasy, and margin erosion. *Journal of Geophysical Research* **96**(B4), 6829–6848.

Moran, K., Backman, J., Brinkhuis, H., Clemens, S. C., Cronin, T. M., Dickens, G. R., Eynaud, F., Gattacceca, J., Jakobsson, M., Jordan, R. W., Kaminski, M., King, J., Koc, N., Krylov, A., Martinez, N., Matthiessen, J., McInroy, D., Moore, T. C., Onodera, J., O'Regan, M., Pälike, H., Rea, B., Rio, D., Sakamoto, T., Smith, D. C., Stein, R. R., St. John, K. E. K., Suto, I., Suzuki, N., Takahashi, K., Watanabe, M., Yamamoto, M., Farrell, J., Frank, M., Kubik, P. W., Jokat, W., Kristoffersen, Y., St John, K., Suto, I., Suzuki, N., Takahashi, K., Watanabe, M., Yamamoto, M., Farrell, J., Frank, M., Kubik, P. W., Jokat, W. & Kristoffersen, Y. 2006. The Cenozoic palaeoenvironment of the Arctic Ocean. *Nature* **441**(7093), 601–5.

Pisias, N. G., Shackleton, N. J. & Hall, M. A. 1985. Stable isotope and calcium carbonate records from hydraulic piston cored hole 574A: High-resolution records from the middle Miocene. In *Initial Reports of the Deep Sea Drilling Project Vol. 85* (eds. L. Mayer & F. Theyer), pp. 735–48. Washington: US Government Printing Office.

Quaijtaal, W., Donders, T. H., Persico, D. & Louwye, S. 2014. Characterising the middle Miocene Mi-events in the Eastern North Atlantic realm: A first high-resolution marine palynological record from the Porcupine Basin. *Palaeogeography, Palaeoclimatology, Palaeoecology* **399**, 140–59.

Schreck, M., Matthiessen, J. & Head, M.J. 2012. A magnetostratigraphic calibration of Middle Miocene through Pliocene dinoflagellate cyst and acritarch events in the Iceland Sea (Ocean Drilling Program Hole 907A). *Review of Palaeobotany and Palynology* **187**, 66–94.

Sexton, P. F. & Wilson, P. A. 2009. Preservation of benthic foraminifera and reliability of deep-sea temperature records: Importance of sedimentation rates, lithology, and the need to examine test wall structure. *Paleoceanography* **24**(2), PA2208.

Sexton, P. F., Wilson, P. A. & Pearson, P. N. 2006. Microstructural and geochemical perspectives on planktic foraminiferal preservation: 'Glassy' versus 'Frosty'. *Geochemistry, Geophysics, Geosystems* **7**(12), Q12P19.

Shackleton, N. J. & Hall, M. A. 1984. Oxygen and carbon isotope stratigraphy of Deep Sea Drilling Project Hole 552a: Plio-Pleistocene glacial history. *Initial Reports of the Deep Sea Drilling Project* **81**, 599–609.

Shackleton, N. J., Hall, M. A. & Boersma, A. 1984. Oxygen and carbon isotope data from Leg 74 foraminifers. *Initial Reports of the Deep Sea Drilling Project* **74**, 599–612.

Shevenell, A. E. & Kennett, J. P. 2004. Paleoceanographic change during the Middle Miocene climate revolution: an Antarctic stable isotope perspective. *Geophysical Monograph Series* **148**, 1–18.

Snyder, S. W. & Waters, V. J. 1984. Cenozoic planktonic foraminiferal biostratigraphy of the Goban Spur Region, Deep Sea Drilling Project Leg 80. In *Initial Reports of the Deep Sea Drilling Project Vol. 80* (eds P. C. de Graciansky & C. W. Poag), pp. 439–72. Washington, DC: US Government Printing Office.

Van Rooij, D., De Mol, B., Huvenne, V., Ivanov, M. & Henriet, J. P. 2003. Seismic evidence of current-controlled sedimentation in the Belgica mound province, upper Porcupine slope, southwest of Ireland. *Marine Geology* **195**(1–4), 31–53.

Williams, G. L., Brinkhuis, H., Pearce, M. A., Fensome, R. A. & Weegink, J. W. 2004. Southern Ocean and global dinflagellate cyst events compared: index events for the Late Cretaceous Neogene. In *Proceedings of the Ocean Drilling Program, Scientific Results Volume 189* (eds N. F. Exon, J. P. Kennett & M. J. Malone), pp. 1–98.

Woodruff, F. & Savin, S. M. 1989. Miocene deepwater oceanography. *Paleoceanography* **4**(1), 87–140.

Woodruff, F. & Savin, S. M. 1991. Mid-Miocene isotope stratigraphy in the deep sea: High-resolution correlations, paleoclimatic cycles, and sediment preservation. *Paleoceanography* **6**(6), 755–806.

Zachos, J., Pagani, M., Sloan, L., Thomas, E. & Billups, K. 2001. Trends, global rhythms, aberrations in global climate 65Ma to present. *Science* **292**(5517), 686–93.